Original Article

TISSUE-ENGINEERED SKELETAL MUSCLE CONSTRUCTED BY HUMAN GINGIVAL FIBROBLASTS

P. Song[1], X.Q. Liu[1], W. Huang[2], F.F. Wang[3], W.J. Li[4], L.M. Zhang[5] and J. Wang[1,*]

[1]Department of Oral Pathology, College and Hospital of Stomatology, Hebei Medical University, The Key Laboratory of Stomatology, 050017 Shijiazhuang, Hebei, China
[2]Department of Oral and Maxillofacial Surgery, School and Hospital of Stomatology, Hebei Medical University, 050017 Shijiazhuang, Hebei, China
[3]Department of Stomatology, The Third Hospital of Hebei Medical University, 050051 Shijiazhuang, Hebei, China
[4]Department of Oral Medicine, The Second Hospital of Hebei Medical University, 050000 Shijiazhuang, Hebei, China
[5]Department of Orthodontics, College and Hospital of Stomatology, Hebei Medical University, 050017 Shijiazhuang, Hebei, China

Abstract

Objective: Tissue engineering technology has achieved remarkable progress in the regenerative repair treatment of many diseases, but the problems in seed cells and scaffold materials are far from being solved. Here, skeletal muscle-like cells (SMLCs) differentiated from human gingival fibroblasts (HGFs) were implanted into bioresorbable collagen membrane (Bio-Gide) scaffold materials to construct tissue-engineered skeletal muscle (TESM), followed by implantation into injured temporal muscle of Beagle dogs to explore the feasibility of constructing TESM and provide new ideas for research on repair and treatment of muscle injuries. **Methods:** HGFs were induced to differentiate into SMLCs by using azacytidine (5-aza). HGFs and SMLCs were identified by immunofluorescence and immunocytochemistry assay. Western blot was used to detect the levels of skeletal muscle cells (SMCs)-associated markers in differentiated HGFs. The SMLCs on Bio-Gide and acellular dermal matrix (ADM) scaffold materials were identified by hematoxylin-eosin (HE) staining and immunocytochemical staining. Transmission electron microscopy (TEM) was used to observe the ultrastructure of SMLCs. The surface ultrastructure of Bio-Gide and ADM scaffolds were observed by scanning electron microscopy (SEM). HE staining and Masson staining were conducted to measure the effects of TESM on the recovery and regeneration of injured skeletal muscle tissues. **Results:** Levels of SMCs-associated markers myosin, myogenic factor 5 (Myf5), and myoblast determination (Myod) in HGFs were the highest at 28 days after treatment with 5-aza. After the induced cells were inoculated on the Bio-Gide scaffold, a large number of cells were attached to the inner surface of the Bio-Gide scaffold, and the cells were in the shape of long columns on the porous and thick collagen, and the cell proliferation was active. The TESM constructed by combining HGFs induced differentiated SMLCs with Bio-Gide scaffolds not only has certain morphological characteristics of skeletal muscle, but also has anti-stress function to a certain extent after culture *in vivo*. **Conclusions:** HGFs have the ability to differentiate into SMLCs, and Bio-Gide is a feasible material for TESM. TESM constructed by combining HGFs induced differentiated SMLCs with Bio-Gide scaffolds facilitated the recovery and regeneration of injured skeletal muscle tissues, thus providing a new idea for the treatment of muscle injury.

Keywords: Human gingival fibroblasts, skeletal muscle-like cells, bioresorbable collagen membrane, tissue-engineered skeletal muscle, injury.

***Address for correspondence**: J. Wang, Department of Oral Pathology, College and Hospital of Stomatology, Hebei Medical University, The Key Laboratory of Stomatology, 050017 Shijiazhuang, Hebei, China. E-mail: wangjie_phd@163.com.

Introduction

The basic autonomous functions of oral and maxillofacial region are inseparable from skeletal muscle contraction [1]. Mature skeletal muscle cells (SMCs) are terminally differentiated cells with weak regenerative ability. Although muscle satellite cells can be activated to participate in the repair of damaged tissues after muscle tissue injury, their number is very limited and cannot meet the needs of tissue regeneration [2,3]. In addition, after skeletal muscle tissue injury, granulation tissue is usually repaired to form scars, which seriously affect motor function. Therefore, building skeletal muscle substitutes to simulate natural skeletal muscle is urgently needed.

Tissue engineering technology (TET) has achieved considerable progress in the regenerative repair treatment of many diseases, including myocardial deficiency, tumors, diabetes, and musculoskeletal regeneration [4–7]. Therefore, the application of tissue-engineered skeletal muscle

(TESM) to repair skeletal muscle defects has become the focus of scholars. The three basic elements of TESM are as follows: acquisition of seed cells, selection of degradable scaffold materials, and cytokines regulating the formation and balance of regenerative tissue [8]. Among them, SMCs (seed cells) play a decisive role in skeletal muscle proliferation and contraction function, but their sources and access are very limited [8]. Therefore, how to obtain a sufficient number of SMCs with certain structure and function is the primary problem to be dealt with in the construction of TESM.

The source of seed cells is very rich, among which the most widely used stem cells, which are not only a kind of cells with self-replicating ability and multi-differentiation potential, but also an immature and incomplete cell, with the function of constructing and regenerating various tissues and organs [9]. Among various types of stem cells, adult stem cells are the most widely used as seed cells for constructing tissue-engineered organs and tissues, including bone marrow mesenchymal stem cells (MSCs), adipose MSCs, human amniotic MSCs and umbilical cord MSCs [10]. However, although these MSCs come from a wide range of sources, their availability in source tissues is very limited, and it is very difficult to obtain high purity MSCs [11]. In addition, MSCs have a series of defects in the process of cell culture, such as early aging problems, lack of specific surface markers during identification, and limited sampling [12,13]. Human gingival fibroblasts (HGFs) are the suitable source of cells for gingival tissue regeneration, and they have the characteristics of wide distribution, convenient sampling, and rapid proliferation [14]. Existing studies have shown that HGFs have similar characteristics to stem cells and multiple differentiation potential, such as osteoblasts, vascular endothelial cells, and vascular smooth muscle cells [15,16]. However, whether HGFs have the potential to differentiate into SMCs has not been clarified.

Previous studies have suggested that the ideal TESM scaffold materials should have good cell-scaffold compatibility, loose and porous structure, ideal surface physicochemical properties, timely degradability, and biomechanical functions, which provide three-dimensional growth space for seed cell growth [17–19]. At present, the commonly used skeletal muscle tissue engineering scaffold materials include synthetic polymer materials and natural biodegradable biological materials. Aliphatic polyester polymers account for the majority of biodegradable synthetic polymers used in skeletal muscle tissue engineering, which has the characteristics of low physiological toxicity, can be degraded at various pH values, has good biocompatibility, can be copolymerized with other monomers to adjust the physical and chemical properties in a wide range, the degradation time is relatively short and controllable, the degradation products can participate in human metabolism and eliminate *in vitro* through normal ways, but the pro-inflammatory reaction after implantation *in vivo* is unavoidable [20,21]. Natural biodegradable biomaterials are derived from animals, plants or human bodies, and have been respected for their good biocompatibility, good degradation performance, and non-toxic degradation products [20]. Among them, the bioresorbable collagen membrane (Bio-Gide) and acellular matrix (ACM) remove the original cellular components, retain the fibrous skeleton and some extracellular matrix components, and have the advantages of no immunogenicity, making them ideal scaffold materials for constructing and repairing oral and maxillofacial defects [20]. Bio-Gide is a double-layer absorbable collagen membrane processed and purified from pig collagen, which not only retains the fiber skeleton and part of the extracellular matrix components but also has the advantages of non-immunogenicity [22]. Bio-Gide is developed specifically for periodontal, peri-implant applications or to improve ossification of bone defects of any origin [23,24]. Another study showed that the matrix in Bio-Gide scaffolds can regulate cell growth factors and promote the adhesion and proliferation of seed cells by activating cell-cell signaling [25]. Acellular dermal matrix (ADM) is a kind of collagen matrix material with three-dimensional spatial structure obtained by removing immunogenic cell components from the epidermis and retaining collagen and other extracellular matrix components in human or animal dermis [26]. Previous studies have shown that ADM can induce vascularization and promote cell growth, has good biocompatibility and low inflammatory response, and is a commonly used scaffold material for oral tissue repair, lymphangiogenesis, abdominal wall reconstruction, and post-mastectomy reconstruction [27–30]. ADM and Bio-Gide scaffolds have been reported to exhibit good mechanical stability [31]. Studies have shown that myoblasts that can differentiate SMCs can be implanted on the surface of synthetic biodegradable scaffolds to mediate skeletal muscle tissue regeneration [32–34]. However, the construction of TESM by inoculating HGF-induced SMCs on Bio-Gide and ADM scaffold materials remains to be clarified.

In this study, skeletal muscle-like cells (SMLCs) differentiated from HGFs were inoculated on Bio-Gide and ADM scaffold materials separately, and the feasibility of constructing TESM *in vitro* was verified. Afterwards, the constructed TESM was implanted in the injured temporal muscle of Beagle dogs to verify the effect of the forces in the animal body on the construction of TESM, providing a new therapeutic approach for the repair and transplantation of skeletal muscle tissue defects.

Materials and Methods

Acquisition of Gum Tissues

Normal gingival tissue specimens of 10 patients aged 20–30 years with impacted tooth extraction were obtained from the Stomatology Hospital of Hebei Medical University. Gingival fiber connective tissues were isolated under sterile conditions for cell culture. The health, rights and pri-

vacy of the subjects were fully protected and the potential risks and harm to the subjects could be minimized. The subjects were explained in detail the process of gingival tissue donation, including the purpose, steps, possible risks, and complications of the surgery.

Cell Culture

The normal gingival tissues of clinically impacted teeth after gingival flap resection were collected and the primary tissue block culture method was used. After the necrotic tissue and residual blood vessels were removed, the tissues were cut into 1 mm × 1 mm tissue blocks and cultured in low glucose-Dulbecco's Modified Eagle's Medium (L-DMEM) containing 15 % fetal bovine serum, 100 U/mL penicillin, and 100 U/mL streptomycin and inverted in an incubator at 37 °C, 5 % CO_2, and 95 % humidity for 4–6 h. The medium was changed every 3–5 days. After the tissue block was firmly attached to the wall, approximately 1–2 mL of culture medium was added to the culture bottle. The culture bottle is slowly flipped over to allow the culture medium to slowly immerse the tissue block, and then placed in the incubator for further cultivation. The medium is changed every 3–5 days. The growth of cells around the tissue blocks was observed under an inverted microscope. When the cells reached 80 % fusion, trypsin digestion was used for cell passage. The logarithmic growth cells were digested, centrifuged, and then cultured in an incubator at 37 °C with 5 % CO_2 saturation humidity. When it was observed under the microscope that the cell protrusions retracted and the gap increased, the cells were removed from the bottle wall by tapping the bottom of the bottle with the hand and complete culture solution was added to terminate digestion. The bottom of the bottle was gently patted with the hand to free the cells from the bottle wall to form a cell suspension, which is passed at 1:4. Additionally, the cells were detected negative by mycoplasma and identified by short-tandem repeat.

Immunofluorescence Staining

Cells (1×10^7 cells/mL) were inoculated into a culture dish preplaced with a treated cover glass. When the cell confluence reaches 70 %–80 %, the cover glass was removed and rinsed with phosphate buffered saline (PBS). The cells were fixed with acetone at 4 °C and blocked at room temperature for 30 min with 5 % normal goat serum to reduce nonspecific binding. Subsequently, the primary antibodies of actin, myosin, vimentin and collagen III were added and incubated for 24 h at 4 °C. After the cells were washed with PBS for three times, secondary antibodies were added and incubated at 37 °C for 30 min, followed by 4′,6-diamidino-2-phenylindole (DAPI) staining for 10 min. 50 % glycerol was added dropwise for sealing. The images were collected and analyzed by laser scanning confocal microscopy.

Immunocytochemistry Staining

After the cells underwent 0.25 % trypsin digestion, they (1×10^7 cells/mL) were inoculated into a culture dish preplaced with a treated cover glass. When the cell confluence reaches 70 %–80 %, the cover glass was removed and rinsed with PBS. The cells were fixed with acetone at 4 °C and incubated with 3 % H_2O_2 for 10 min to block endogenous peroxidase. Afterwards, the primary antibodies of actin, myosin, vimentin and collagen III were added and incubated for 24 h at 4 °C. After the cells were washed with PBS for three times, secondary antibodies were added and incubated at 37 °C for 1 h, followed by 3,3′-diaminobenzidine (DAB) staining for 10 min, hematoxylin re-staining, gradient alcohol dehydration, transparentizing with xylene, sealing tablets, and microscopic observation.

Selection of 5-aza Concentration and Time for Induction

5-aza was added into the medium with concentrations of 0 μg/mL, 5 μg/mL, 10 μg/mL and 20 μg/mL, respectively, and the relevant indicators were detected after 4 weeks of induction. The induction fluid is changed every three days.

After the optimal induction concentration of 5-aza was determined, HGFs were induced by L-DMEM containing the concentration of 5-aza for 0, 7, 14, 21, 28, and 35 days separately. Cell induction was observed daily, and the induction fluid was changed every 2 days. The morphological changes in SMLCs were observed under an inverted microscope and SMCs-associated markers were detected.

Western Blot Assay

Proteins were isolated from cells by radioimmunoprecipitation assay lysis buffer and then quantified by bicinchoninic acid method. The protein samples of each group were 100 μg. The total proteins were separated by sodium dodecyl sulfate-polyacrylamide gel electrophoresis. Then, the proteins were transferred to polyvinylidene fluoride membranes. Subsequently, the membranes were sealed with 5 % skim milk to avoid excessive non-specific color development. After the primary antibodies were incubated at 4 °C overnight, the membranes were incubated with the second antibodies for 2 h at room temperature. Afterwards, an appropriate amount of electrochemiluminescence developer was added for strip color development. The target bands were analyzed with ImageJ analysis software (1.43, NIH, Bethesda, MD, USA), and the relative protein levels were measured by the ratio of protein to the internal reference glyceraldehyde-3-phosphate dehydrogenase.

Observation of the Ultrastructure of Induced Cells

After 28 days of 5-aza induction, the induced SMLCs were digested, prepared into 2×10^6 cells/mL cell suspension, and then centrifuged for 10 min at 3000 rpm/min. The cells were first fixed with 2.5 % glutaraldehyde for 4 h and then fixed with 1 % osmium tetroxide (OsO_4) for 2 h, fol-

lowed by dehydrating with gradient acetone for 15 min at 4 °C. Subsequently, the samples were encapsulated in a capsule or plate with an embedding agent and aggregated in the oven at 37 °C for 24 h and 60 °C for 48 h. The samples were cut into ultrathin slices with a thickness of 50 nm by an ultrathin microtome and then re-dyed with uranyl acetate for 30–45 min and lead citrate for 5–30 min. The ultrathin sections were placed on a small copper mesh, and the ultrastructure of SMLCs was observed under transmission electron microscopy (TEM, H-7500, Hitachi, Tokyo, Japan).

Preparation of Bio-Gide and ADM Scaffold Materials

After 24 h of aseptic PBS immersion, Bio-Gide and ADM scaffold materials were soaked in isopropyl alcohol for 30 min and then washed 10 times with PBS. After being dried in a sterile super clean table, they were irradiated by ultraviolet lamp for 2 h. Before the seed cells were planted, the Bio-Gide and ADM scaffold materials were soaked in DMEM complete culture solution at 37 °C and 5 % CO_2 overnight and then cut to 5 × 5 mm size for use.

Hematoxylin-Eosin (HE) Staining

After being fixed with 4 % formalin, samples were embedded in paraffin and then cut into slices (5 μm thickness). The paraffin sections were dewaxed and hydrated according to the process of xylene-gradient ethanol-water. Afterwards, the slices were stained with hematoxylin solution for 5 min, followed by 0.5 % eosin solution for 3 min. Then, the slices were dehydrated with gradient ethanol, transparentized with xylene, and mounted with resin. The morphological of the tissues were observed under an optical microscope (BX-53, Olympus, Tokyo, Japan).

Observation of Scaffold Surface Structure and Inoculation of SMLCs

Scaffolds with or without SMLCs were fixed in 2.5 % glutaraldehyde at 4 °C for 24 h, followed by ethanol gradient dehydration, tert-butanol drying, bonding, and coating. Afterwards, the scaffolds' surface structure and the inoculation of SMLCs were observed under scanning electron microscopy (SEM).

Immunohistochemistry Staining

The obtained tissue engineering graft was implanted in 4 % neutral formalin for fixation, dehydrated and transparent treatment, impregnated with wax, and fixed on a microtome for sectioning with a thickness of 8 μm, and finally dewaxed. The specific methods of immunohistochemistry staining were similar to those of immunocytochemistry staining.

Measurement of Scaffold Water Absorption

The Bio-Gide and ADM materials were weighed before and after immersion in PBS, and the weight (W) was marked W0 in the dry state and W1 after soaking for 24 h. The percentage of water absorption of the support material was calculated as follows: (W1 – W0)/W0 × 100%.

Measurement of the Mechanical Properties of Scaffolds

The Zwick/Roell Z020 universal mechanical test machine (Berlin, Germany) was used to measure tensile strength, including breaking strength and elongation at break, and record stress and strain. The experiment was divided into three groups, namely the skeletal muscle (muscle) group, ADM group, and Bio-Gide group for detection. The two ends of the sample were fixed on the mechanical test machine, and the sample was kept moist with PBS during the whole experiment. All samples should be pre-adjusted before the test. The sample length was 1 cm and was stretched at 10 mm/min until the specimen was pulled apart. Stress and strain were recorded. Stress is the mechanical state that describes the internal points of the object in all directions. The internal force received per unit area is the stress. Strain is the amount that describes the shape change of a material under the action of external forces. Stress-strain curves were plotted with stress as the ordinate and strain as the abscissa. The breaking strength and elongation at break were calculated.

Breaking strength = the maximum stress/cross-sectional area at which the material breaks

Elongation at break (%) = the displacement value of the material at the time of tensile break/the original length of the material

Measurement of Scaffold Pressure Blasting

A pressure gun was applied to measure the pressure blasting. In brief, a pressure gun filled with saline was connected to one end of the support material, and the other end of the support material was sealed with a clamp. Then, the pressure regulator was slowly rotated to increase the water pressure until the support material burst, at which time the reading was recorded.

Cell Counting Kit-8 (CCK-8) Assay the Cytotoxicity of Scaffold Materials

The samples to be tested were divided into two groups, Bio-Gide group and ADM group, and placed in 96-well plates with 100 μL cell suspension. The culture plates were cultured in incubators at 5 % CO_2 and 37 °C for 24, 48, and 72 h. After the fresh medium was changed, 10 μL of CCK-8 solution was added to each well. After the culture plate was incubated for 4 h, the absorbance (A) at 450 nm was measured by an enzyme-labeled instrument. Cytotoxic activity (%), i.e., relative growth rate (RGR) = (A (scaffold) – A (blank)/A (no scaffold) – A (blank)) × 100 %

A (scaffold): absorbance of well with cells, CCK-8 solution, and scaffold material

A (blank): absorbance of well with medium and CCK-8 solution but no cells

A (no scaffold): absorbance of well with cells, CCK-8 solution and no scaffold material

In accordance with the RGR value, cytotoxicity was evaluated as follows:

RGR ≥75 %, cytotoxicity grade 0 or 1, qualified.

RGR was 50 %–74 %, and the cytotoxicity was grade 2, which should be combined with the comprehensive evaluation of cell morphology.

RGR ≤49 %, cytotoxicity grades 3–5, unqualified.

Animal

The skeletal muscle of the face of rodents is relatively small, and we selected the temporal muscle of Beagle dogs to greatly restore the similarity of human chewing muscle. Although Beagles are worth a lot of money, we feel that larger animals are more maneuverable. Twelve healthy male Beagle dogs were purchased from Beijing Maas Biological Co., Ltd. (Beijing, China). They were aged 10–12 months, weighed about 11 or 12 kg, and had no systemic diseases. The Beagle dogs were kept in the Laboratory Animal Center of Hebei Medical University, were fed quantitatively two times every morning and evening, and drank freely. After 1 month of adaptive feeding, the experiment was carried out. This experiment used Beagle dogs as the model, and the number was determined by statistical calculation to ensure the minimum amount of use. Beagle dogs were kept in a standard environment with proper temperature, humidity and light, adequate food and water, and regular cleaning of cages. In the experimental procedure, the Beagle dogs received anesthesia and analgesia, the surgery was performed by trained personnel, and monitored closely afterward. The end point of the experiment was clear and euthanasia was carried out if necessary. The experimental personnel were all trained and qualified. The experiments strictly abided by the national and institutional animal testing regulations and policies.

The Beagle dogs were fasted to water 12 h before surgery. 30 min before surgery, 0.07–0.08 mL/kg of Su Mian Xin II (0.1 g/mL) was injected into the hind leg muscles of the dogs for sedation. Then, 1 % pentobarbital sodium was given intramuscular injection of 0.3 mL/kg for further anesthesia. According to the anesthesia status, 1 % pentobarbital sodium was administered intramuscularly at a dose of 0.3 mL/kg every 2 h for anesthesia maintenance. Then, 0.5 % lidocaine hydrochloride was injected into the local infiltration of the surgical area to assist in maintaining the anesthesia effect. After the experimental Beagle dogs entered a state of general anesthesia, they were fixed on the operating table and disinfected with iodine and alcohol in the surgical area. All surgical instruments were disinfected and sterilized under high temperature and pressure. An aseptic hole towel was applied to create defect wounds of about 5 × 5 mm in the temporal area under local anesthesia, and sterile surgical suture was performed. The right temporal muscles of 12 Beagle dogs were well preserved, and they served as the normal control group. Four Beagle dogs had left temporal muscle injuries, which were directly sutured and treated. Four Beagle dogs had left temporal muscle injuries, which were repaired with empty scaffolds (Bio-Gide) and sutured. Four Beagle dogs had left temporal muscle injuries, which were repaired with Bio-Gide-tissue-engineered skeletal muscle (TESM) and sutured. The entire surgical procedure was proficiently performed by the same experimenter, strictly adhering to the principle of sterility. Soft food was given within 1 day after surgery. Antibiotics were injected for 1 week, the wound was treated with decompression and bandaging, and the Beagle dog's head was treated with special headgear. After the operation, each Beagle dog was observed regularly for any abnormality in feeding, mental state, stool, and daily activities. After 2 weeks, the Beagle dogs were killed by air embolization under general anesthesia (similar to anesthesia during operation). Temporal muscle tissue specimens were taken out from each group of Beagle dogs and divided into three parts. One part was fixed in 10 % neutral formalin for HE staining and Masson staining identification, another part was fixed in 2.5 % glutaraldehyde for scanning electron microscopic observation, and another part was used for pressure bearing determination.

Masson Staining

After being fixed, samples were embedded in paraffin and then cut into slices. Dewaxing was performed after paraffin sections were made. The sections were then stained with Masson complex dye solution for 5 min. After being soaked in 0.2 % acetic acid solution, the sections were stained with 5 % phosphotungstic acid for 10 min, followed by bright green solution for 5 min. After 0.2 % acetic acid washing, the sections were dehydrated with gradient ethanol and transparentized with xylene for 10 min. The slices were sealed with neutral gum, observed and photographed under a light microscope.

Statistical Analysis

Data were expressed as the mean ± standard deviation. Animal experiments were conducted on four samples per group. Cell scaffold related experiments were conducted with five samples per group. Each experiment was independently repeated three times. The data followed a normal distribution. One-way analysis of variance followed by Tukey's post-hoc test was applied for comparisons between multiple groups, and student's *t*-test was applied for comparisons between two groups. SPSS (version 17.0, SPSS Inc., Chicago, IL, USA) statistical software was used for statistical analysis. Values of $p < 0.05$ were regarded as statistically significant.

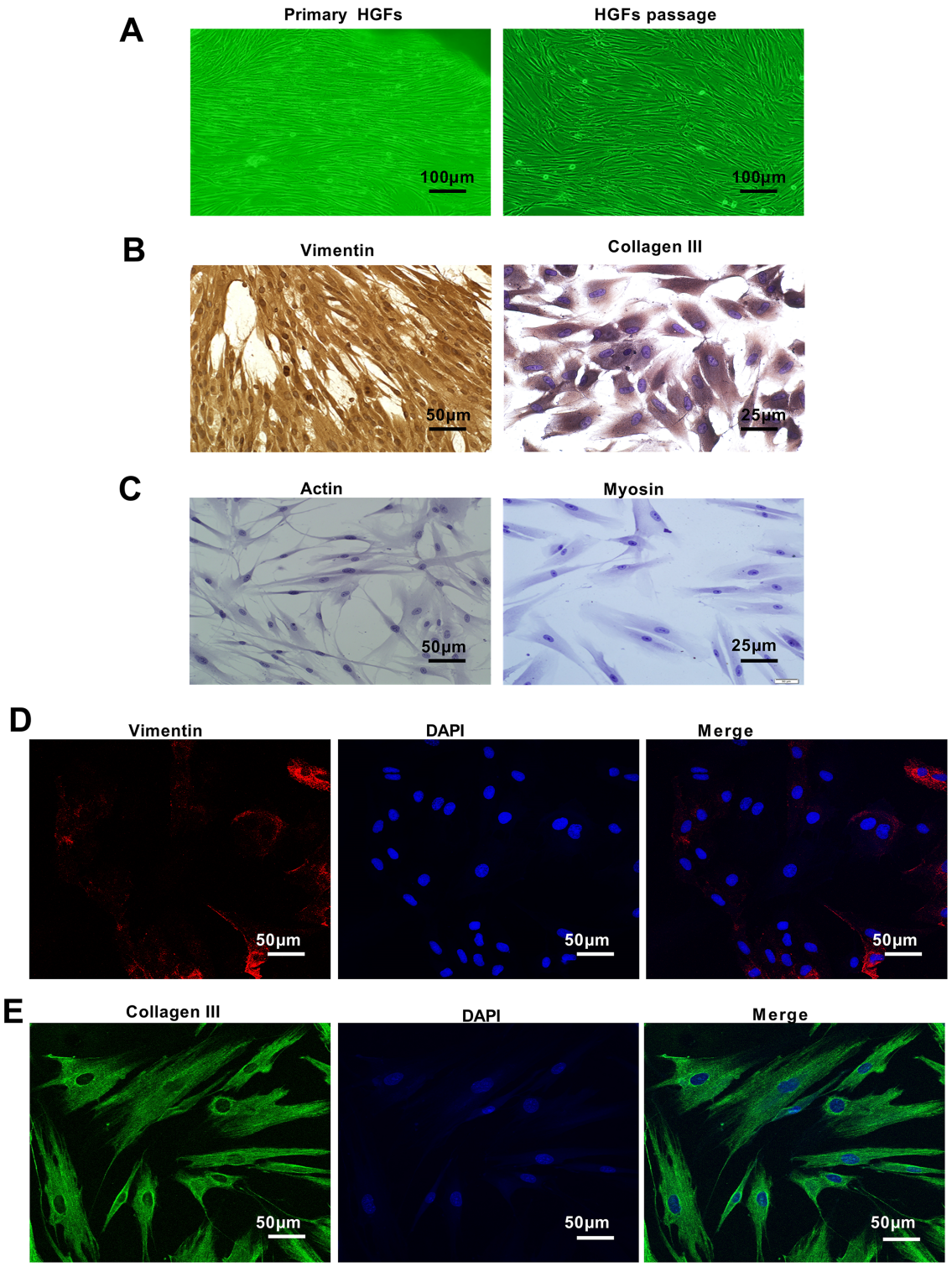

Fig. 1. Morphological observation and identification of primary HGFs. (**A**) Morphological of primary culture and passage of HGFs observed by immunofluorescence staining (scale bar: 100 μm). (**B**) Positive expressions of vimentin and collagen III in the cytoplasm of HGFs were detected by immunocytochemical staining (scale bar: 25 and 50 μm). (**C**) Negative expressions of actin and myosin in the cytoplasm of HGFs were detected by immunocytochemical staining (scale bar: 25 and 50 μm). (**D,E**) Positive expression levels of vimentin and collagen III in the cytoplasm of HGFs were observed by immunofluorescence staining (scale bar: 50 μm). HGFs, human gingival fibroblasts; DAPI, 4′,6-diamidino-2-phenylindole.

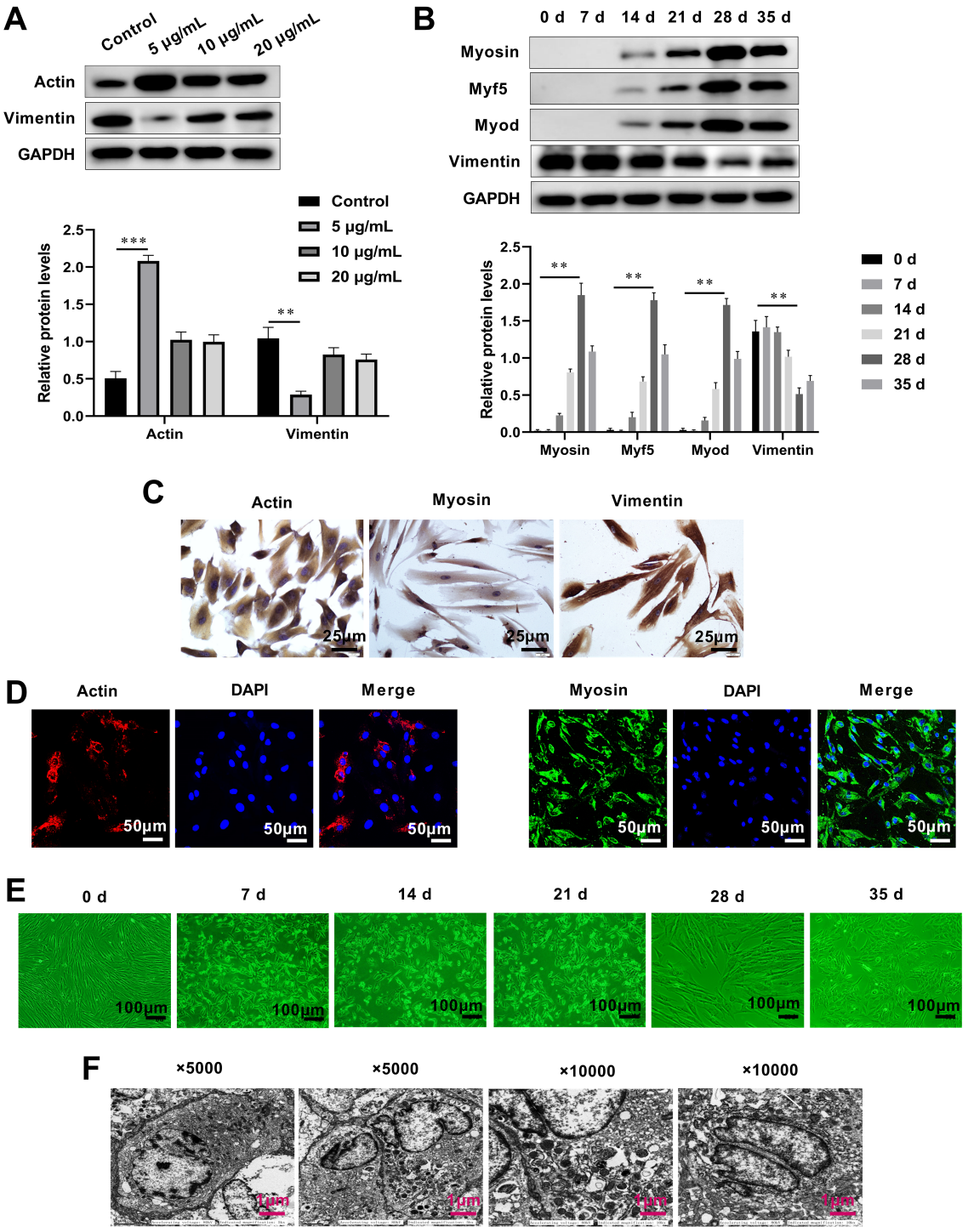

Fig. 2. Expression of SMCs-related markers in differentiated HGFs. (**A**) Expression of vimentin and actin in HGFs treated with various concentrations of 5-aza. (**B**) Western blot analysis of vimentin, myosin, Myf5, and Myod protein levels in HGFs treatment with 5 μg/mL of 5-aza at various time points. (**C**) Positive expressions of actin, myosin, and vimentin in the cytoplasm of HGFs were detected by immunocytochemical staining (scale bar: 25 μm). (**D**) Positive expressions of actin and myosin in the cytoplasm of HGFs were detected by immunofluorescence staining (scale bar: 50 μm). (**E**) Differentiation of HGFs into SMLCs by 5 μg/mL of 5-aza at various time points (scale bar: 100 μm). (**F**) Ultrastructure of SMLCs from HGFs induced by 5-aza was observed by TEM with different magnification (scale bar: 1 μm). $^{**}p < 0.01$; $^{***}p < 0.001$. SMCs, skeletal muscle cells; SMLCs, skeletal muscle-like cells; Myf5, myogenic factor 5; Myod, myoblast determination; GAPDH, internal reference glyceraldehyde-3-phosphate dehydrogenase; DAPI, 4′,6-diamidino-2-phenylindole; TEM, transmission electron microscopy.

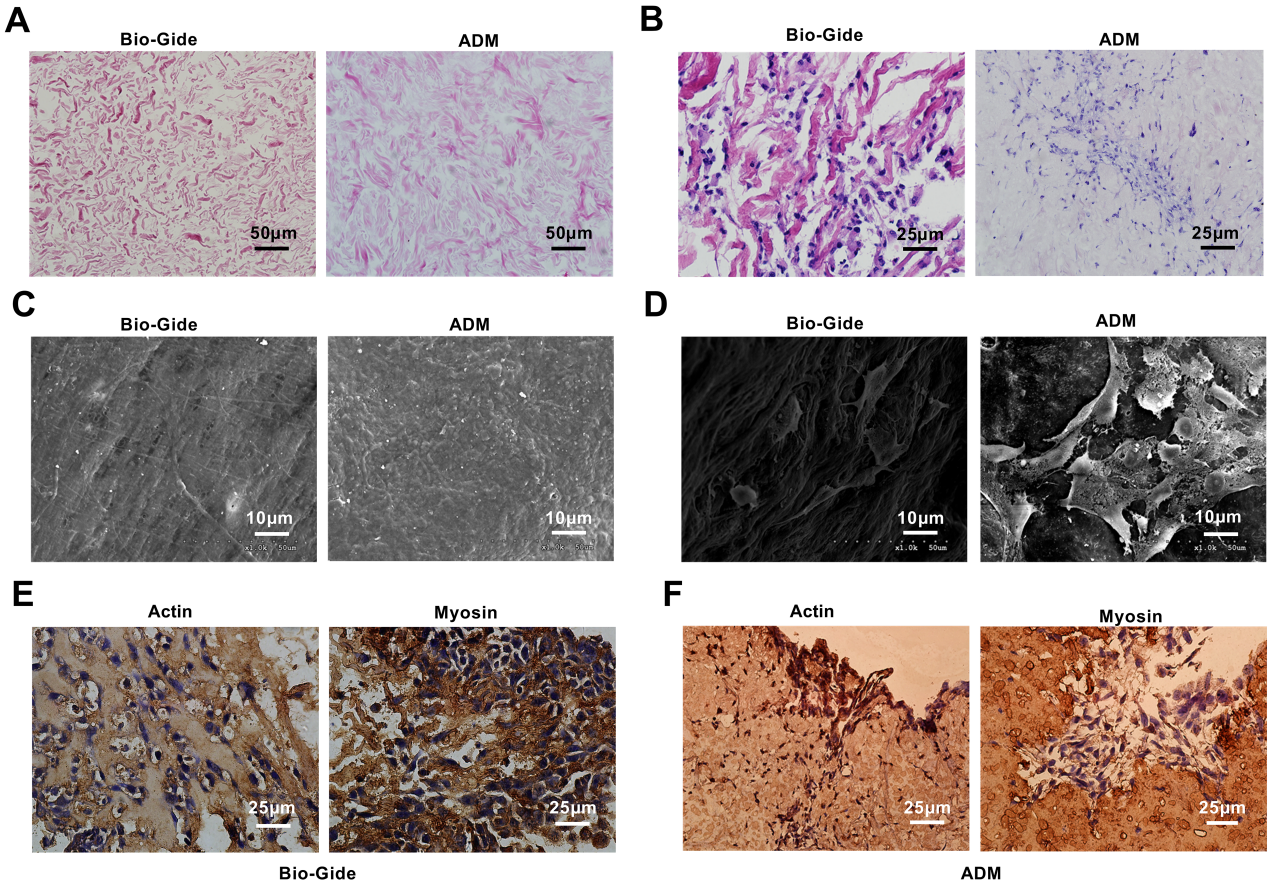

Fig. 3. Construction of TESM *in vitro*. (**A**) Surface structures of Bio-Gide and ADM scaffold materials were analyzed by HE staining (scale bar: 50 μm). (**B**) SMLCs growing on the surface and internal of Bio-Gide and ADM scaffold materials were detected by HE staining (scale bar: 25 μm). (**C**) Surface ultrastructures of Bio-Gide and ADM scaffold materials were observed by SEM (scale bar: 10 μm). (**D**) SMLCs growing on the surface and internal of Bio-Gide and ADM scaffold materials were observed by SEM (scale bar: 10 μm). (**E**,**F**) Immunohistochemistry observation showed that actin and myosin were positively expressed in the cytoplasm of SMLCs on the surface and internal of Bio-Gide and ADM scaffold materials (scale bar: 25 μm). TESM, tissue-engineered skeletal muscle; HE, hematoxylin-eosin; Bio-Gide, bioresorbable collagen membrane; ADM, acellular dermal matrix; SEM, scanning electron microscopy.

Results

Morphological Observation and Identification of Primary HGFs

An inverted microscope was used to observe the morphology of HGFs, and the results showed that the HGFs were arranged in bundles or swirls, and the cells had radiative growth centered on tissue blocks (Fig. 1**A**). The growth of cultured cells was satisfactory, reaching 90 %–100 % in 3 or 4 days (Fig. 1**A**). Subsequently, the primary HGFs were immunostained with vimentin, collagen III, actin, and myosin antibodies. The immunocytochemistry results displayed that the vimentin and collagen III proteins were positively expressed (Fig. 1**B**), whereas the actin and myosin proteins were negatively expressed in HGFs (Fig. 1**C**). Meanwhile, immunofluorescence staining also showed that the vimentin and collagen III proteins were positively expressed in HGFs (Fig. 1**D,E**). These results indicate that HGFs could be used for follow-up experimental research.

Expression of SMCs-Related Markers in Differentiated HGFs

5-aza was used to induce HGF differentiation into SMCs, and the optimal 5-aza concentration and induced differentiation time of HGFs to SMLCs were explored. The HGFs were treated with different concentrations of 5-aza (5, 10, and 20 μg/mL). After 28 days, the HGF- and SMCs-associated markers were determined by Western blot assay. The results showed that the level of vimentin significantly decreased, whereas that of actin increased after treatment with 5-aza (5, 10, and 20 μg/mL) compared with the control group. The vimentin protein level was lowest, whereas the actin level was the highest after treatment with 5 μg/mL of 5-aza (Fig. 2**A**). Subsequently, the cells were treated with 5 μg/mL of 5-aza for 0, 7, 14, 21, 28, and 35 days separately. The Western blot results showed that the relative levels of SMC-associated markers (myosin, myogenic factor 5 (Myf5), and myoblast determination (Myod))

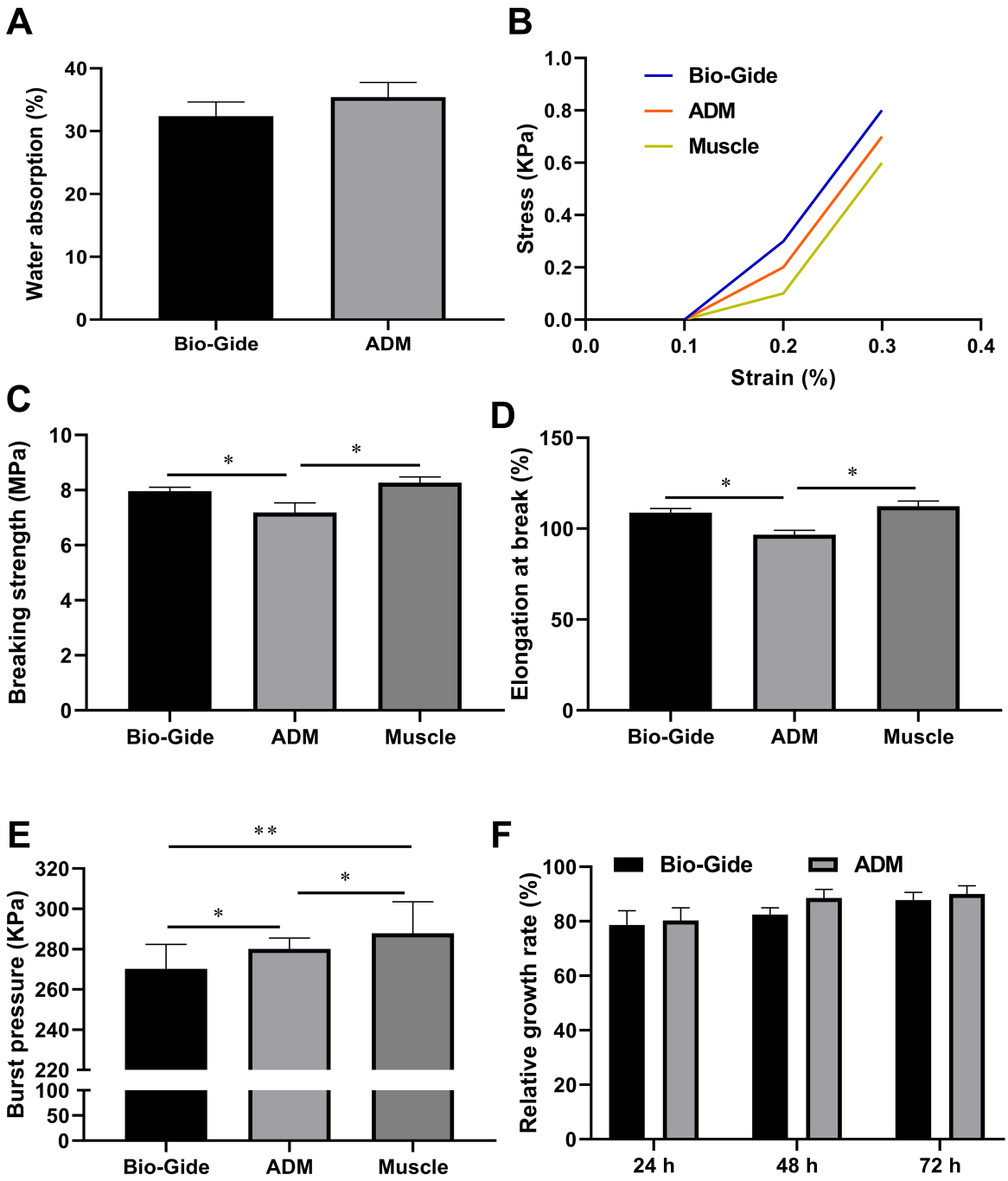

Fig. 4. Feasibility analysis of constructing TESM. (**A**) Comparison of water absorption between Bio-Gide and ADM scaffold materials. (**B**) Stress-strain curves of Bio-Gide scaffold, ADM scaffold, and muscle tissues. **(C,D)** Breaking strength, and elongation at break of Bio-Gide scaffold, ADM scaffold, and muscle tissues were detected by Zwick/Roell Z020 universal mechanical test machine. (**E**) Burst pressure of Bio-Gide scaffold, ADM scaffold, and muscle tissues was compared. (**F**) Cytotoxicity of Bio-Gide and ADM scaffolds was analyzed by CCK-8. *$p < 0.05$; **$p < 0.01$. CCK-8, cell counting kit-8.

were the highest at 28 days (Fig. 2**B**). The immunocytochemistry and immunofluorescence results displayed that the actin and myosin proteins were positively expressed in cells after 28 days of induction (Fig. 2**C,D**). Morphological observation showed that after 14 days of induction, most of the cells were still arranged in bundles or swirls (Fig. 2**E**). At 28 days, the morphology of the cells changed from long spindle to columnar or rod-like, the cells enlarged and thickened, and the two ends of the cells became blunt (Fig. 2**E**). At 35 days, most of the cells were columnar or rod-

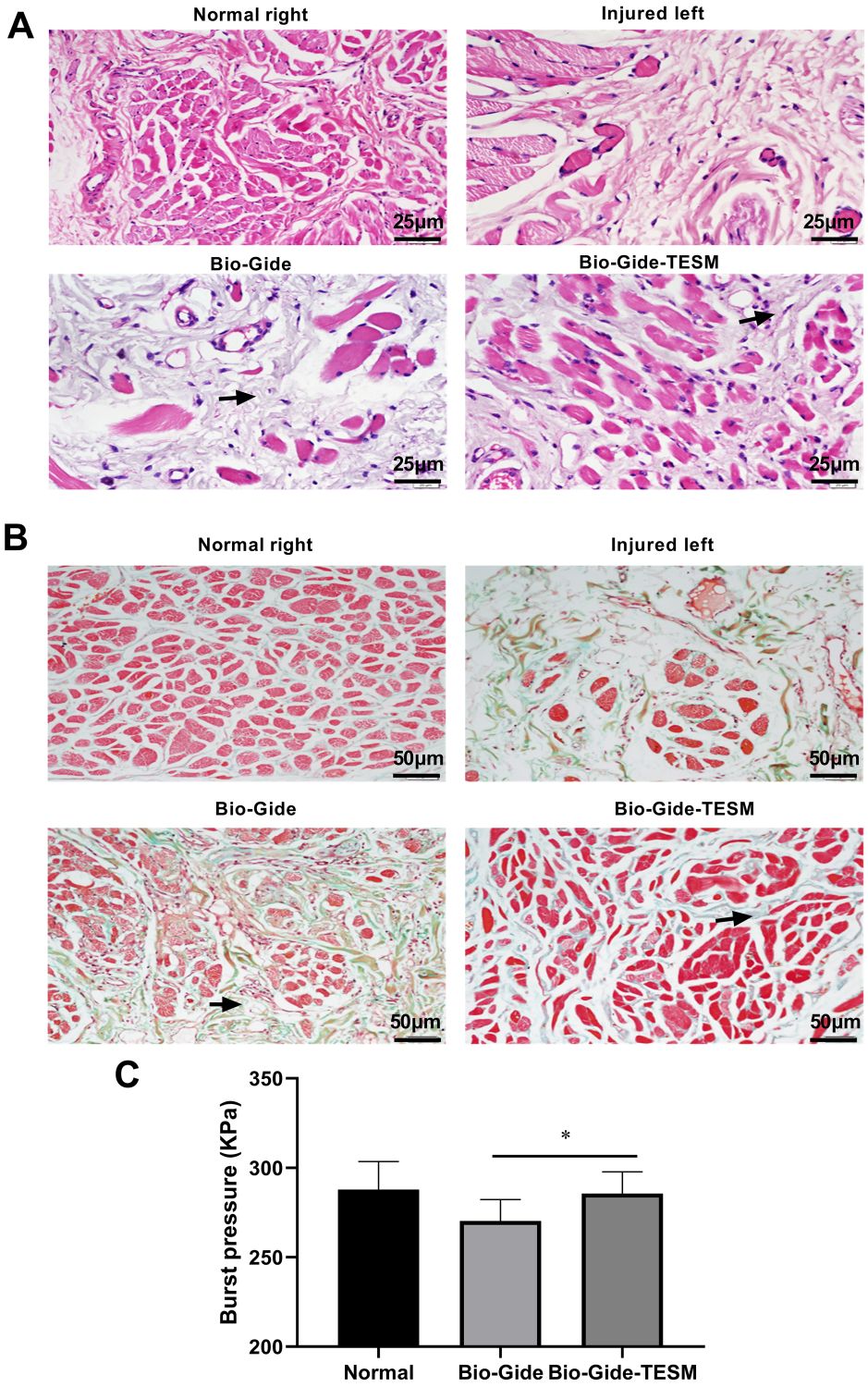

Fig. 5. Effects of TESM constructed by combining HGFs induced differentiated SMLCs with Bio-Gide scaffolds on repair and regeneration of injured skeletal muscle tissues. (**A,B**) The morphological changes of the left injured temporal muscle of Beagle dogs after Bio-Gide-TESM implantation for 2 weeks were observed by HE staining (scale bar: 25 μm) and Masson staining (scale bar: 50 μm). (**C**) Comparison of burst pressure in Bio-Gide scaffold, Bio-Gide-TESM, and muscle tissues. The area indicated by the arrow was the region of muscle regeneration and scaffold degradation. *$p < 0.05$.

shaped, with a large number of cells proliferating and some cells fusing, which was consistent with normal SMC morphology (Fig. 2**E**). The TEM results showed that the nucleus was located in the center of the cell, and many mitochondria, Golgi complexes, and some dense structures were found in the cytoplasm, but no transverse features, which was different from the structure of real SMCs (Fig. 2**F**). These results suggest that the optimal concentration of 5-aza and induced differentiation time for inducing HGF differentiation into SMLCs were 5 μg/mL and 28 days. Moreover, these results indicate that SMLCs differentiated from HGFs have morphological and immunological characteristics of SMCs.

Construction of TESM In Vitro

Next, the SMLCs were inoculated on Bio-Gide and ADM scaffold materials, and the scaffold materials and cell attachment were analyzed. HE staining and SEM were applied for observing the surface ultrastructure of scaffold materials and the inoculation of SMLCs on the scaffold materials. The results from HE revealed that the Bio-Gide scaffold was composed of collagen fibers and matrix without any cellular structure, the fibers in the scaffold were arranged in layers, and the fiber structure was sparse (Fig. 3**A**). The ADM scaffold was composed of collagen fibers and matrix without any cellular structure, and the fibers in the scaffold were densely arranged (Fig. 3**A**). A large amount of SMLCs were attached to the inner surface of the Bio-Gide scaffold, growing in dispersed layers along the surface and internal fibers (Fig. 3**A**). The SMLCs planted on the surface of the ADM scaffold were well grown, were arranged in layers, and grew on the surface of the scaffold, with a small number of cells growing into the scaffold (Fig. 3**B**). The SEM results showed that the inner surface of the Bio-Gide scaffold displayed very sparse and thick collagen fibers with loose layers and some porous structures on the surface (Fig. 3**C**). The fibers of the ADM scaffold were dense, with few pores and uniform distribution (Fig. 3**C**). The induced SMLCs grew in layers along the fibers on the inner surface of the Bio-Gide scaffold material, and the cell arrangement was relatively dispersed, but the cell to cell was connected into a network structure, and the induced SMLCs grew in a layered manner on the inner surface of the ADM scaffold (Fig. 3**D**). The immunohistochemistry results suggested that the actin and myosin proteins were positively expressed in the SMLCs planted in the Bio-Gide and ADM scaffold materials, and the positive rate in the Bio-Gide scaffold was higher than that in the ADM scaffold (Fig. 3**E,F**). These results suggest that the structural characteristics of Bio-Gide scaffold materials could provide a structural basis for improving the success rate of implantation cells.

Feasibility Analysis of Constructing TESM

Subsequently, the water absorption, mechanical strength, and tensile stress of the scaffold materials were analyzed. The results showed no significant difference in water absorption capacity between the Bio-Gide and ADM scaffold materials (Fig. 4**A**). The stress-strain curves showed that Bio-Gide and ADM scaffolds have higher tensile resistance than normal muscles (Fig. 4**B**). Besides, the fracture strength and elongation at break of the Bio-Gide scaffold were similar to that of skeletal muscle, whereas those of the ADM scaffold were lower (Fig. 4**C,D**). The burst pressure of the Bio-Gide scaffold material was smaller than that of the ADM scaffold material and skeletal muscle (Fig. 4**E**). CCK-8 assay was applied to access the cytotoxicity of the Bio-Gide and ADM scaffold materials. The results showed that the number of SMLCs on the Bio-Gide and ADM scaffold materials gradually increased at 24, 48, and 72 h, and the relative growth rate was above 75 % (Fig. 4**F**), indicating that the cytotoxicity grade was 1, and the toxicity test was qualified. These results indicate that the absorbable Bio-Gide scaffold material can be used as the carrier and living environment of SMLCs to construct TESM successfully.

Effects of TESM Constructed by Combining HGFs Induced Differentiated SMLCs with Bio-Gide Scaffolds on Repair and Regeneration of Injured Skeletal Muscle Tissues

To further validate the feasibility of constructing TESM with HGFs combined with Bio-Gide materials, the constructed TESM was implanted in the injured temporal muscle of Beagle dogs to evaluate the function of TESM *in vivo*. After 2 weeks, the results from HE staining and Masson staining showed that the scaffold began to degrade, the structure disappeared, and a large number of matrix components and a small amount of skeletal muscle fiber hyperplasia were present at the defect site in the empty scaffold group (Fig. 5**A,B**, the area indicated by the arrow). In the TESM group, the scaffold began to degrade, the structure disappeared, a large number of muscle fiber hyperplasia were present at the scaffold site, neovascularization began, a new skeletal muscle tissue was formed in some areas, and inflammatory cell infiltration was hardly visible (Fig. 5**A,B**, the area indicated by the arrow). Moreover, the burst pressure of the Bio-Gide-TESM group was higher than that of the Bio-Gide scaffold group, and no significant difference was observed in the burst pressure between the Bio-Gide-TESM group and the normal muscle group (Fig. 5**C**). These results suggest that the constructed TESM promoted the repair and regeneration of injured skeletal muscle tissues.

Discussion

The regeneration and repair ability of human skeletal muscle tissue is notoriously low. Currently, autogenous bone transplantation, allogeneic bone transplantation, and synthetic substitute are mainly used to repair bone defects and nonunion, but they are difficult to meet the needs of clinical repair of various bone defects [35]. TET has been

reported to open up a new research and application field for the clinical repair of skeletal muscle tissue defects, and it has become one of the most promising tissue engineering achievements in clinical application [8]. Brookes *et al.* [36] demonstrated that functional three-dimensional tissue engineering skeletal muscles could be developed from primary skeletal muscle progenitor cells and standardized oligomeric collagen for laryngeal reconstruction. Das *et al*. [37] created a bioengineered structure by combining nerve cells and muscle cells on a bionic scaffold, which improved the recovery of voluble muscle loss. The present study demonstrated that HGFs have the ability to differentiate into SMLCs, and Bio-Gide is a feasible material for TESM. HGF-constructed TESM facilitated the recovery and regeneration of injured skeletal muscle tissues, thus providing a new idea for the treatment of muscle injury.

A previous study has found that after muscle injury, the MSCs at the injury site differentiate into muscle satellite cells, which can promote muscle repair and regeneration [38]. Another study found that 5-aza could induce rabbit MSCs to differentiate into cells with skeletal muscle characteristics [39]. However, the defects of MSCs such as senescence in the early stage of culture and lack of specific surface markers in identification limit their wide application [12,13]. A previous study proposed that periodontal membrane fibroblasts have differentiation potential and the characteristics of stem cells [40]. Hu *et al*. [41] believed that the human periodontal ligament cell (hPDLC) cultured by direct tissue block method is a heterogeneous cell population containing stem cell components. Another study showed that the derived cells from hPDL tissue contained a certain proportion of stem cells [42]. In the present study, HGFs were used as the induced differentiation cells to investigate whether they could differentiate into SMCs after induction by 5-aza.

5-aza is known to have a demethylation effect, and the methylation site contains a site that regulates myogenic differentiation and is in the phase of transcriptional inactivation [43]. Previous studies have shown that 5-aza can induce MSCs to differentiate into cardiomyocytes [44,45]. In the present study, 5-aza was used to induce the differentiation of HGFs into SMCs, and the optimal differentiation concentration and differentiation time of 5-aza were determined. SMCs' specific surface marker is well known to be actin, while myosin, Myf5, and Myod are also specifically expressed in SMCs [46]. The Western blot results showed that the levels of actin, myosin, Myf5, and Myod were the highest after differentiation at 28 days by 5 μg/mL of 5-aza. The results from TEM demonstrated that the differentiated cells contained some typical organelles, and a large number of dense structures could be seen in the cytoplasm. These findings suggested that the SMLCs formed by 5 μg/mL 5-aza-induced differentiation of HGFs for 28 days showed morphological and immunological characteristics of SMCs.

The Bio-Gide scaffold has been reported to be a commonly used scaffold material to guide tissue regeneration. Schlegel *et al*. [22] reported that Bio-Gide membranes are promising new tools for dental surgery and guided bone regeneration in humans. Another research discovered that porous tantalum and Bio-Gide collagen membrane with bone marrow MSCs repaired full-layer joint defects in patients with femoral head necrosis [47]. Camelo *et al*. [48] demonstrated that autogenous bone in combination with porous bone mineral matrix, together with Bio-Gide collagen membrane, can stimulate substantial new bone and cementum formation. Luczyszyn *et al*. [49] showed that ADM was used as a membrane associated with absorbable hydroxyapatite for bone regeneration. Zhou *et al*. [50] demonstrated that ADM is a safe and effective biomedical material for surgical defect repair and pharyngeal function reconstruction of hypopharyngeal carcinoma. However, the results showed that compared with the ADM scaffold material, the SMLCs inoculated with Bio-Gide scaffold material proliferated significantly, indicating that the structural characteristics of the Bio-Gide scaffold material enhanced the number of cell adhesion. The stress, breaking strength, and elongation at break of the Bio-Gide scaffold were similar to those of a normal skeletal muscle. This finding confirmed that the Bio-Gide scaffold had similar physical and chemical properties to a normal skeletal muscle, indicating the feasibility of Bio-Gide as a TESM scaffolds.

In skeletal muscle injuries, tissue engineering represents a biological alternative for replacement of large tissue loss after severe damage. A previous study showed that when myoblasts bound to a three-dimensional fibrin matrix were injected into the injured rat muscle area, the fibrin carrier did not cause an inflammatory response and allowed myoblasts to integrate into the host muscle fibers [51]. Fibrin scaffolds have also been combined with adult cells for muscle regeneration after extensive tissue loss in a mouse model of tibialis anterior defect [52]. Collagen scaffolds have shown the ability to induce skeletal muscle-like tissue regeneration, and the scaffold structure is able to support the mechanical forces generated in the muscle tissue [53]. To verify the effect of the forces in the animal body on the constructed TESM, the constructed TESM *in vitro* was implanted in the injured temporal muscle of Beagle dogs and used as a bioreactor for dynamic enhancement culture experiment in the animal body. In the present study, most of the scaffolds were degraded after 2 weeks of implantation in the injured temporal muscle of Beagle dogs, a large number of muscle fibers showed hyperplasia, neovascularization began, and a new skeletal muscle tissue was formed in some areas. Moreover, TESM formed by human HGFs induced differentiation into SMLCs implanted in Bio-Gide scaffolds has anti-stress function, to some extent, after culture *in vivo*.

Conclusions

HGFs have the ability to differentiate into SMLCs, and Bio-Gide is a feasible scaffold material for TESM. The TESM constructed by HGFs facilitated the recovery and regeneration of injured skeletal muscle tissues. Gingival fibroblasts have the advantages of active self-renewal ability, strong repair and healing ability, convenient extraction, less trauma, high survival rate *in vitro*, and can differentiate into SMLCs under appropriate stimulation, which has broad research prospects. It not only provides a new source of skeletal muscle seed cells, but also provides a new way to repair muscle defects with TESM in clinical application. However, more experimental and clinical studies are needed to confirm its role in skeletal muscle regeneration before it can be widely used.

List of Abbreviations

SMLCs, skeletal muscle-like cells; HGFs, human gingival fibroblasts; Bio-Gide, bioresorbable collagen membrane; TESM, tissue-engineered skeletal muscle; ADM, acellular dermal matrix; HE, hematoxylin-eosin; TEM, transmission electron microscopy; Myf5, myogenic factor 5; Myod, myoblast determination; SMCs, skeletal muscle cells; TET, tissue engineering technology; L-DMEM, low glucose-Dulbecco's Modified Eagle's Medium; DAB, 3,3′-diaminobenzidine; PBS, phosphate buffered saline; OsO_4, osmium tetroxide; CCK-8, cell counting kit-8; A, absorbance; RGR, relative growth rate; W, weight; SEM, scanning electron microscopy; GAPDH, internal reference glyceraldehyde-3-phosphate dehydrogenase; DAPI, 4′,6-diamidino-2-phenylindole; hPDLC, human periodontal ligament cell; MSCs, mesenchymal stem cells.

Availability of Data and Materials

The dataset that supported the results and findings of this research is available from the corresponding author on reasonable request.

Author Contributions

PS implemented the project, drafted the manuscript. XQL directed the experiment, project expansion, and software support. WH assisted in the implementation of projects, and performed animal experiments. FFW & WJL assisted in the implementation of projects, and performed basic experiments. LMZ was responsible for statistical analysis and data acquisition. JW conceptualized and designed research, reviewed article, and contacted the magazine editor. All authors reviewed it critically for important intellectual content. All authors read and approved the final manuscript. All authors agreed to be accountable for all aspects of the work in ensuring that questions related to the accuracy or integrity of any part of the work were appropriately investigated and resolved.

Ethics Approval and Consent to Participate

This study has been approved by the Ethics Committee of Stomatology Hospital of Hebei Medical University (No. 2020032). All the subjects signed informed consent. The animal feeding and experimental procedures used in this study were in accordance with the Stomatology Hospital of Hebei Medical University Animal Experiment management rules (No. 2020014).

Acknowledgments

Not applicable.

Funding

This research was supported by the 2021 Hebei Medical Science Research Project Plan (No. 20210413).

Conflict of Interest

The authors declare no conflict of interest.

References

[1] Rot I, Kablar B. Role of skeletal muscle in palate development. Histology and Histopathology. 2013; 28: 1–13. https://doi.org/10.14670/HH-28.1.

[2] Dumont NA, Bentzinger CF, Sincennes MC, Rudnicki MA. Satellite Cells and Skeletal Muscle Regeneration. Comprehensive Physiology. 2015; 5: 1027–1059. https://doi.org/10.1002/cphy.c140068.

[3] Persson PB. Skeletal muscle satellite cells as myogenic progenitors for muscle homoeostasis, growth, regeneration and repair. Acta Physiologica. 2015; 213: 537–538. https://doi.org/10.1111/apha.12451.

[4] Wang Z, Wang L, Li T, Liu S, Guo B, Huang W, *et al*. 3D bioprinting in cardiac tissue engineering. Theranostics. 2021; 11: 7948–7969. https://doi.org/10.1016/j.actbio.2018.08.026.

[5] Ma H, Feng C, Chang J, Wu C. 3D-printed bioceramic scaffolds: From bone tissue engineering to tumor therapy. Acta Biomaterialia. 2018; 79: 37–59. https://doi.org/10.1016/j.actbio.2018.08.026.

[6] Soetedjo AAP, Lee JM, Lau HH, Goh GL, An J, Koh Y, *et al*. Tissue engineering and 3D printing of bioartificial pancreas for regenerative medicine in diabetes. Trends in Endocrinology and Metabolism: TEM. 2021; 32: 609–622. https://doi.org/10.1016/j.tem.2021.05.007.

[7] Ye B, Wu B, Su Y, Sun T, Guo X. Recent Advances in the Application of Natural and Synthetic Polymer-Based Scaffolds in Musculoskeletal Regeneration. Polymers. 2022; 14: 4566. https://doi.org/10.3390/polym14214566.

[8] Jiang XK, Yang JY, Zhang M. Research status of tissue engineering techniques in repairing skeletal muscle injury. Medical Journal of Chinese People's Liberation Army. 2022; 4: 394–401.

[9] Xue J, Liu Y. Mesenchymal Stromal/Stem Cell (MSC)-Based Vector Biomaterials for Clinical Tissue Engineering and Inflammation Research: A Narrative Mini Review. Journal of Inflammation Research. 2023; 16: 257–267. https://doi.org/10.2147/JIR.S396064.

[10] Gonzalez-Vilchis RA, Piedra-Ramirez A, Patiño-Morales CC, Sanchez-Gomez C, Beltran-Vargas NE. Sources, Characteristics, and Therapeutic Applications of Mesenchymal Cells in Tissue Engineering. Tissue Engineering and Regenerative Medicine. 2022; 19: 325–361. https://doi.org/10.1007/s13770-021-00417-1.

[11] Zhou T, Yuan Z, Weng J, Pei D, Du X, He C, *et al*. Challenges and advances in clinical applications of mesenchymal stromal cells. Journal of Hematology & Oncology. 2021; 14: 24. https://doi.org/10.1186/s13045-021-01037-x.

[12] Weng Z, Wang Y, Ouchi T, Liu H, Qiao X, Wu C, *et al*. Mesenchymal Stem/Stromal Cell Senescence: Hallmarks, Mechanisms, and Combating Strategies. Stem Cells Translational Medicine. 2022; 11: 356–371. https://doi.org/10.1093/stcltm/szac004.

[13] Lv FJ, Tuan RS, Cheung KM, Leung VY. Concise review: the surface markers and identity of human mesenchymal stem cells. Stem Cells. 2014; 32: 1408–1419. https://doi.org/10.1002/stem.1681.

[14] Asad MM, Abdelhafez RS, Barham R, Abdaljaleel M, Alkurdi B, Al-Hadidi S, *et al*. Three-dimensional cultures of gingival fibroblasts on fibrin-based scaffolds for gingival augmentation: A proof-of-concept study. Archives of Oral Biology. 2023; 154: 105754. https://doi.org/10.1016/j.archoralbio.2023.105754.

[15] Rutherford RB, Moalli M, Franceschi RT, Wang D, Gu K, Krebsbach PH. Bone morphogenetic protein-transduced human fibroblasts convert to osteoblasts and form bone *in vivo*. Tissue Engineering. 2002; 8: 441–452. https://doi.org/10.1089/107632702760184709.

[16] Liu X, Wang J, Dong F, Li H, Hou Y. Induced differentiation of human gingival fibroblasts into VSMC-like cells. Differentiation; Research in Biological Diversity. 2017; 95: 1–9. https://doi.org/10.1016/j.diff.2017.01.001.

[17] Sbrana F, Fotia C, Bracalello A, Baldini N, Marletta G, Ciapetti G, *et al*. Multiscale characterization of a chimeric biomimetic polypeptide for stem cell culture. Bioinspiration & Biomimetics. 2012; 7: 046007. https://doi.org/10.1088/1748-3182/7/4/046007.

[18] Carnes ME, Pins GD. Skeletal Muscle Tissue Engineering: Biomaterials-Based Strategies for the Treatment of Volumetric Muscle Loss. Bioengineering. 2020; 7: 85. https://doi.org/10.3390/bioengineering7030085.

[19] Koning M, Harmsen MC, van Luyn MJA, Werker PMN. Current opportunities and challenges in skeletal muscle tissue engineering. Journal of Tissue Engineering and Regenerative Medicine. 2009; 3: 407–415. https://doi.org/10.1002/term.190.

[20] Huang W, Liao H. Research progress of scaffold materials in skeletal muscle tissue engineering. Zhongguo Xiu Fu Chong Jian Wai Ke Za Zhi = Zhongguo Xiufu Chongjian Waike Zazhi = Chinese Journal of Reparative and Reconstructive Surgery. 2010; 24: 1386–1391.

[21] Sicari BM, Londono R, Badylak SF. Strategies for skeletal muscle tissue engineering: seed vs. soil. Journal of Materials Chemistry. B. 2015; 3: 7881–7895. https://doi.org/10.1039/c5tb01714a.

[22] Schlegel AK, Möhler H, Busch F, Mehl A. Preclinical and clinical studies of a collagen membrane (Bio-Gide). Biomaterials. 1997; 18: 535–538. https://doi.org/10.1016/s0142-9612(96)00175-5.

[23] Oortgiesen DA, Plachokova AS, Geenen C, Meijer GJ, Walboomers XF, van den Beucken JJ, *et al*. Alkaline phosphatase immobilization onto Bio-Gide® and Bio-Oss® for periodontal and bone regeneration. Journal of Clinical Periodontology. 2012; 39: 546–555. https://doi.org/10.1111/j.1600-051X.2012.01877.x.

[24] Allan B, Ruan R, Landao-Bassonga E, Gillman N, Wang T, Gao J, *et al*. Collagen Membrane for Guided Bone Regeneration in Dental and Orthopedic Applications. Tissue Engineering. Part A. 2021; 27: 372–381. https://doi.org/10.1089/ten.TEA.2020.0140.

[25] Papaioannou KA, Markopoulou CE, Gioni V, Mamalis AA, Vayouraki HN, Kletsas D, *et al*. Attachment and proliferation of human osteoblast-like cells on guided bone regeneration (GBR) membranes in the absence or presence of nicotine: an *in vitro* study. The International Journal of Oral & Maxillofacial Implants. 2011; 26: 509–519.

[26] Fosnot J, Kovach SJ 3rd, Serletti JM. Acellular dermal matrix: general principles for the plastic surgeon. Aesthetic Surgery Journal/the American Society for Aesthetic Plastic Surgery. 2011; 31: 5S–12S. https://doi.org/10.1177/1090820X11417576.

[27] Xu X, Cui N, Wang E. Application of an acellular dermal matrix to a rabbit model of oral mucosal defects. Experimental and Therapeutic Medicine. 2018; 15: 2450–2456. https://doi.org/10.3892/etm.2018.5705.

[28] Cherubino M, Pellegatta I, Tamborini F, Cerati M, Sessa F, Valdatta L. Evaluation of lymphangiogenesis in acellular dermal matrix. Indian Journal of Plastic Surgery: Official Publication of the Association of Plastic Surgeons of India. 2014; 47: 318–324. https://doi.org/10.4103/0970-0358.146578.

[29] Patel KM, Bhanot P. Complications of acellular dermal matrices in abdominal wall reconstruction. Plastic and Reconstructive Surgery. 2012; 130: 216S–224S. https://doi.org/10.1097/PRS.0b013e318262e186.

[30] Tierney BP, De La Garza M, Jennings GR, Weinfeld AB. Clinical Outcomes of Acellular Dermal Matrix (SimpliDerm and AlloDerm Ready-to-Use) in Immediate Breast Reconstruction. Curēus. 2022; 14: e22371. https://doi.org/10.7759/cureus.22371.

[31] Qiu YL, Chen X, Hou YL, Hou YJ, Tian SB, Chen YH, *et al*. Characterization of different biodegradable scaffolds in tissue engineering. Molecular Medicine Reports. 2019; 19: 4043–4056. https://doi.org/10.3892/mmr.2019.10066.

[32] Shen Z, Guo S, Ye D, Chen J, Kang C, Qiu S, *et al*. Skeletal muscle regeneration on protein-grafted and microchannel-patterned scaffold for hypopharyngeal tissue engineering. BioMed Research International. 2013; 2013: 146953. https://doi.org/10.1155/2013/146953.

[33] Mulbauer GD, Matthew HWT. Biomimetic Scaffolds in Skeletal Muscle Regeneration. Discoveries. 2019; 7: e90. https://doi.org/10.15190/d.2019.3.

[34] Jo HJ, Kang MS, Heo HJ, Jang HJ, Park R, Hong SW, *et al*. Skeletal muscle regeneration with 3D bioprinted hyaluronate/gelatin hydrogels incorporating MXene nanoparticles. International Journal of Biological Macromolecules. 2024; 265: 130696. https://doi.org/10.1016/j.ijbiomac.2024.130696.

[35] Tolstunov L. Maxillary tuberosity block bone graft: innovative technique and case report. Journal of Oral and Maxillofacial Surgery: Official Journal of the American Association of Oral and Maxillofacial Surgeons. 2009; 67: 1723–1729. https://doi.org/10.1016/j.joms.2009.03.043.

[36] Brookes S, Voytik-Harbin S, Zhang H, Halum S. Three-dimensional tissue-engineered skeletal muscle for laryngeal reconstruction. The Laryngoscope. 2018; 128: 603–609. https://doi.org/10.1002/lary.26771.

[37] Das S, Browne KD, Laimo FA, Maggiore JC, Hilman MC, Kaisaier H, *et al*. Pre-innervated tissue-engineered muscle promotes a pro-regenerative microenvironment following volumetric muscle loss. Communications Biology. 2020; 3: 330. https://doi.org/10.1038/s42003-020-1056-4.

[38] Archacka K, Grabowska I, Mierzejewski B, Graffstein J, Górzyńska A, Krawczyk M, *et al*. Hypoxia preconditioned bone marrow-derived mesenchymal stromal/stem cells enhance myoblast fusion and skeletal muscle regeneration. Stem Cell Research & Therapy. 2021; 12: 448. https://doi.org/10.1186/s13287-021-02530-3.

[39] Sheng X, Feng J, Wu S, Jin L, Yu X, Zhang B. Differentiation of rabbit bone marrow mesenchymal stem cells into myogenic cells *in vitro* and expression of vascular endothelial growth factor gene after transfection. Di 1 Jun Yi Da Xue Xue Bao = Academic Journal of the First Medical College of PLA. 2004; 24: 290–294.

[40] Sokos D, Everts V, de Vries TJ. Role of periodontal ligament fibroblasts in osteoclastogenesis: a review. Journal of Periodontal Research. 2015; 50: 152–159. https://doi.org/10.1111/jre.12197.

[41] Hu B, Zhang Y, Zhou J, Li J, Deng F, Wang Z, *et al*. Low-intensity pulsed ultrasound stimulation facilitates osteogenic differentiation of human periodontal ligament cells. PloS One. 2014; 9: e95168. https://doi.org/10.1371/journal.pone.0095168.

[42] Seo BM, Miura M, Gronthos S, Bartold PM, Batouli S, Brahim J, *et al*. Investigation of multipotent postnatal stem cells from human periodontal ligament. Lancet. 2004; 364: 149–155. https://doi.org/10.1016/S0140-6736(04)16627-0.

[43] Fei W, Pang E, Hou L, Dai J, Liu M, Wang X, *et al*. Synergistic Effect of Hydrogen and 5-Aza on Myogenic Differentiation through the p38 MAPK Signaling Pathway in Adipose-Derived Mesenchymal Stem Cells. International Journal of Stem Cells. 2023; 16: 78–92. https:

//doi.org/10.15283/ijsc21238.

[44] Cao F, Niu LL, Meng L, Zhao LX, Zheng M, Yue W, *et al*. Cardiomyocyte-like differentiation of human bone marrow mesenchymal stem cells after exposure of 5-azacytidine *in vitro*. Shi Yan Sheng Wu Xue Bao. 2004; 37: 118–124.

[45] Liu Y, Song J, Liu W, Wan Y, Chen X, Hu C. Growth and differentiation of rat bone marrow stromal cells: does 5-azacytidine trigger their cardiomyogenic differentiation? Cardiovascular Research. 2003; 58: 460–468. https://doi.org/10.1016/s0008-6363(03)00265-7.

[46] Le Ricousse-Roussanne S, Larghero J, Zini JM, Barateau V, Foubert P, Uzan G, *et al*. *Ex vivo* generation of mature and functional human smooth muscle cells differentiated from skeletal myoblasts. Experimental Cell Research. 2007; 313: 1337–1346. https://doi.org/10.1016/j.yexcr.2007.01.022.

[47] Liu B, Yang F, Wei X, Zhang X, Zhang Y, Wang B, *et al*. An exploratory study of articular cartilage and subchondral bone reconstruction with bone marrow mesenchymal stem cells combined with porous tantalum/Bio-Gide collagen membrane in osteonecrosis of the femoral head. Materials Science & Engineering. C, Materials for Biological Applications. 2019; 99: 1123–1132. https://doi.org/10.1016/j.msec.2019.02.072.

[48] Camelo M, Nevins ML, Lynch SE, Schenk RK, Simion M, Nevins M. Periodontal regeneration with an autogenous bone-Bio-Oss composite graft and a Bio-Gide membrane. International Journal of Periodontics & Restorative Dentistry. 2001; 21: 109–119.

[49] Luczyszyn SM, Papalexiou V, Novaes AB Jr, Grisi MF, Souza SL, Taba M Jr. Acellular dermal matrix and hydroxyapatite in prevention of ridge deformities after tooth extraction. Implant Dentistry. 2005; 14: 176–184. https://doi.org/10.1097/01.id.0000165082.77499.41.

[50] Zhou Y, Zhang Z, Chen H, Liu J, Lin R. Application of acellular dermal matrix to reconstruct the defects after hypopharyngeal carcinoma resection. American Journal of Otolaryngology. 2021; 42: 102847. https://doi.org/10.1016/j.amjoto.2020.102847.

[51] Beier JP, Stern-Straeter J, Foerster VT, Kneser U, Stark GB, Bach AD. Tissue engineering of injectable muscle: three-dimensional myoblast-fibrin injection in the syngeneic rat animal model. Plastic and Reconstructive Surgery. 2006; 118: 1113–1121. https://doi.org/10.1097/01.prs.0000221007.97115.1d.

[52] Page RL, Malcuit C, Vilner L, Vojtic I, Shaw S, Hedblom E, *et al*. Restoration of skeletal muscle defects with adult human cells delivered on fibrin microthreads. Tissue Engineering. Part A. 2011; 17: 2629–2640. https://doi.org/10.1089/ten.TEA.2011.0024.

[53] Kroehne V, Heschel I, Schügner F, Lasrich D, Bartsch JW, Jockusch H. Use of a novel collagen matrix with oriented pore structure for muscle cell differentiation in cell culture and in grafts. Journal of Cellular and Molecular Medicine. 2008; 12: 1640–1648. https://doi.org/10.1111/j.1582-4934.2008.00238.x.

Editor's note: The Scientific Editor responsible for this paper was Kai Zheng.

Received: 11th December 2024; **Accepted**: 19th March 2025; **Published**: 26th May 2025